REPORT DOCUMENTATION PAGE

Form Approved
OMB No. 0704-0188

1. REPORT DATE *(DD-MM-YYYY)*	**2. REPORT TYPE**	**3. DATES COVERED** *(From - To)*
January 2013	Journal Article	January 2013- February 2013

4. TITLE AND SUBTITLE
Thermophysical Properties of Energetic Ionic Liquids/Nitric Acid Mixtures: Insights from Molecular Dynamics Simulations

5a. CONTRACT NUMBER
FA9300-11-C-3012

5b. GRANT NUMBER

5c. PROGRAM ELEMENT NUMBER

6. AUTHOR(S)

Justin B. Hooper, Grant D. Smith, and Dmitry Bedrov

5d. PROJECT NUMBER

5e. TASK NUMBER

5f. WORK UNIT NUMBER
QOPX

7. PERFORMING ORGANIZATION NAME(S) AND ADDRESS(ES)

Air Force Research Laboratory (AFMC)
AFRL/RQRP
10 E. Saturn Blvd.
Edwards AFB CA 93524-7680

8. PERFORMING ORGANIZATION REPORT NO.

9. SPONSORING / MONITORING AGENCY NAME(S) AND ADDRESS(ES)
Air Force Research Laboratory (AFMC)
AFRL/RQR
5 Pollux Drive
Edwards AFB CA 93524-7048

10. SPONSOR/MONITOR'S ACRONYM(S)

11. SPONSOR/MONITOR'S REPORT NUMBER(S)
AFRL-RQ-ED-JA-2013-031

12. DISTRIBUTION / AVAILABILITY STATEMENT
Distribution A: Approved for Public Release; Distribution Unlimited. PA#13159

13. SUPPLEMENTARY NOTES
N/A

14. ABSTRACT

Molecular dynamics (MD) simulations of mixtures of the room temperature ionic liquids (ILs) 1-butyl-4 methyl imidazolium [BMIM]/dicyanoamide [DCA] and [BMIM][NO3---] with HNO3 have been performed utilizing the polarizable, quantum chemistry based APPLE&P® potential. Experimentally it has been observed that [BMIM][DCA] exhibits hypergolic behavior when mixed with HNO3 while [BMIM][NO3---] does not. The structural, thermodynamic and transport properties of the IL/HNO3 mixtures have been determined from equilibrium MD simulations over the entire composition range (pure IL to pure HNO3) based on bulk simulations. Additional (non---equilibrium) simulations of the composition profile for IL/HNO3 interfaces as a function of time have been utilized to estimate the composition dependent mutu al diffusion coefficients for the mixtures. The latter have been employed in continuum---level simulations in order to examine the nature (composition and width) of the IL/HNO3 interfaces on the millisecond time scale.

15. SUBJECT TERMS

16. SECURITY CLASSIFICATION OF:			**17. LIMITATION OF ABSTRACT**	**18. NUMBER OF PAGES**	**19a. NAME OF RESPONSIBLE PERSON**
					G. Vahjiani
a. REPORT	**b. ABSTRACT**	**c. THIS PAGE**	SAR	31	**19b. TELEPHONE NO** *(include area code)*
Unclassified	**Unclassified**	**Unclassified**			661-525-5657

Standard Form 298 (Rev. 8-98)
Prescribed by ANSI Std. 239.18

Thermophysical Properties of Energetic Ionic Liquids/Nitric Acid Mixtures: Insights from Molecular Dynamics Simulations

Justin B. Hooper, Grant D. Smith, and Dmitry Bedrov

Wasatch Molecular, Incorporated

825 N. 300 W., Salt Lake City, UT 84103

Abstract

Molecular dynamics (MD) simulations of mixtures of the room temperature ionic liquids (ILs) 1-butyl-4-methyl imidazolium [BMIM]/dicyanoamide [DCA] and [BMIM][NO_3^-] with HNO_3 have been performed utilizing the polarizable, quantum chemistry based APPLE&P® potential. Experimentally it has been observed that [BMIM][DCA] exhibits hypergolic behavior when mixed with HNO_3 while [BMIM][NO_3^-] does not. The structural, thermodynamic and transport properties of the IL/HNO_3 mixtures have been determined from equilibrium MD simulations over the entire composition range (pure IL to pure HNO_3) based on bulk simulations. Additional (non-equilibrium) simulations of the composition profile for IL/HNO_3 interfaces as a function of time have been utilized to estimate the composition dependent mutual diffusion coefficients for the mixtures. The latter have been employed in continuum-level simulations in order to examine the nature (composition and width) of the IL/HNO_3 interfaces on the millisecond time scale.

I. Introduction

There is increasing interest in use of room temperature ionic liquids (ILs) as fuels and propellants. Particularly enticing is the fact that RTILs have negligible vapor pressure, making them intrinsically much safer than traditional high vapor pressure and toxic fuels such as hydrazine. While most IL fuels are not hypergolic (i.e., do not spontaneously combust) when mixed with a liquid oxidizer (e.g., nitric acid), there is a number of energetic ILs that do exhibit hypergolicity.[1] Amongst these are 1-butyl-4-methyl imidazolium [BMIM]/dicyanoamide [DCA], shown in Figure 1. While [BMIM][DCA] when mixed with HNO_3 is hypergolic, [BMIM][NO_3^-] is not.[2,3] Understanding the behavior of any hypergolic system is very challenging and complicated due to the large manifold of reactions involved and the complex interplay between thermophysical properties and chemical kinetics. When a fuel droplet comes in contact with an oxidizer, some initial mixing is followed by the exothermic pre-ignition reactions that begin to decompose both fuel and oxidizer, producing various gaseous products. The pathways for these reactions involve highly reactive transient species that are difficult to detect experimentally. Changes in temperature and species concentrations due to these reactions as well as the underlying chemical kinetics themselves are also strongly dependent on physical factors that determine heat and mass transfer in these systems. Thermophysical properties such as enthalpy of mixing, species inter-diffusion, and thermal conductivity can all play an important role in controlling energy dissipation during the pre-ignition reaction stage.[2,4]

While thermophysical and transport properties of [BMIM][DCA] and [BMIM][NO_3^-] have been investigated both experimentally[5-10] and from MD simulations,[11-18] there are no data available about thermophysical properties of these liquids mixed with HNO_3. Taking into account that it usually takes multiple milliseconds for ignition to occur in a hypergolic system there is a significant

(from a molecular scale point of view) time period when thermodynamic and thermophysical processes are dominating the behavior of the mixture and influence the kinetics of initial reactions. Therefore, we have carried out atomistic molecular dynamics (MD) simulations of HNO_3/[BMIM][DCA] and HNO_3/[BMIM][NO_3^-] mixtures for the purposes of better quantifying the thermophysical properties of these mixtures with the ultimate aim of understanding the nature of hypergolicity in ILs. Furthermore, modeling of HNO_3/[BMIM][DCA], whether at the continuum level or at the level of detailed liquid-phase reaction pathways, will benefit greatly from an improved understanding of the thermodynamics, structure and transport properties of the mixture.

II. Force Field and Simulation Methodology

MD simulations was performed using the polarizable APPLE&P® force field that has been developed and extensively validated on a variety of substances including ILs[19] and slightly modified for application to the specific ILs studied here.[11] Using this force field our previous simulations showed very good agreement with experimental thermophysical data for pure [BMIM][DCA] and [BMIM][NO_3^-] RTILs.[11] For the current study the force field for HNO_3 was obtained using our standard procedure, which considered all non-bonded interactions and the dipole polarizability of all atoms to be as transferred from previously calculated quantities for the nitrate anion, while bond, angular, and dihedral interactions were fit from *ab initio* data obtained at the MP2//aug-cc-pvDz level. Specific details about our fitting procedure can be found in Ref. [19] while the complete set of force field parameters is available free of charge upon signing a user license agreement.

MD simulations of bulk [BMIM][NO_3^-]/HNO_3 and [BMIM][DCA]/HNO_3 mixtures have been conducted at 333 K and atmospheric pressure using cubic simulation cell (see Fig. 1). Systems with a composition ranging from 0.0 to 1.0 mol fraction IL in steps of 0.2 have been simulated. The pure HNO_3 system contained 512 molecules while the mixed systems employed 600, 560, 512, or 468

total molecules in order of increasing IL mol fraction. Pure IL data was taken from the previous work, which employed 150 ionic pairs.[11] For the mixed systems, the number of ionic pairs employed were 100, 160, 192, and 208 for the mole fractions studied in increasing IL concentration. MD simulations were conducted using the molecular simulation package Lucretius which has the capability to handle polarization effects. Covalent bond lengths were constrained using the velocity-Verlet form of the SHAKE algorithm.[20] The Ewald summation method was used for treatment of long-range electrostatic forces between partial atomic charges and between partial charges and induced dipoles. A tapering function was used to drive the induced dipole/induced dipole interactions to zero at the cutoff of 10 Å, with scaling starting at 9.3 Å. (The form of the tapering function is given in the Supporting Information) Induced dipoles were calculated *via* a direct iteration with a predictor corrector method. A cutoff of 10 Å was used for all van der Waals interactions and the real part of electrostatic interactions in the Ewald summation. A multiple time step reversible reference system propagator algorithm[21] was employed. A time step of 0.5 fs was used for bonding, bending, dihedral, and out-of-plane deformation motions, while a 1.5 fs time step was used for non-bonded interactions within cutoff radius of 6.0 Å. Finally, the non-bonded interactions in the range between 6.0 and 10.0 Å and reciprocal part of electrostatic interactions were updated every 3 fs. Each system was initially equilibrated in the NPT ensemble for at least 1 ns, while production runs ranged from 120 to 180 ns depending on the system and temperature. The length of the production run was chosen to be long enough to allow molecules to reach a diffusive regime (when the ion mean squared displacement shows a linear time dependence, $MSD(t) \sim t$), therefore allowing an accurate estimation of the self-diffusion coefficients.

In addition to equilibrium bulk simulations of IL/HNO_3 mixtures described above we also conducted MD simulations at non-equilibrium conditions in which we monitor the process of intermixing of IL and HNO_3 liquids. To conduct these simulations a liquid-liquid interface has to be set up as also shown in Figure 1 where RTIL and oxidizer are well separated. Several adjustments

to the simulation protocol have been implemented to allow these types of simulations. First, since IL and oxidizer are miscible the preparation of initial configuration that allows sharp yet tight (no vacuum) interface between IL and oxidizer has to be prepared. To create a sharp liquid-liquid interface we modify parameters for van der Waals interactions between IL and oxidizer molecules to make them more repulsive. Specifically, we set dispersion parameters C_{ij} (of the term $-C_{ij}/r^6$) to zero for all cross-terms interactions between the IL and oxidizer. This simple modification was enough to provide a sharp interface between liquids without creating any additional artifacts to bulk materials away from the interface. Using this approach, initial configurations can be equilibrated for any period of time and then switched to simulations with realistic force field for production runs sampling the intermixing rate. In these simulations, the simulation cell dimensions were 35 X 35 X 140 Å with the larger dimension being perpendicular to the interface. Systems contained approximately the same volume of IL and oxidizer. During these simulations the pressure (stress tensor) was controlled separately in each direction, allowing the simulation to account for changes in pressure associated with mixing of the components. Simulations were conducted at 333 K and atmospheric pressure control along the large dimension (perpendicular to the interface). Two other dimensions were fixed at 35x35.

III. Simulations of Bulk Mixtures

A. Structure

We began our analysis of the HNO_3/IL mixtures by investigating liquid-phase structure as a function of mixture composition. Figures 2a-b show center-of-mass BMIM-BMIM radial distribution functions g(r) as a function of separation r for HNO_3/[BMIM][DCA] and HNO_3/[BMIM][NO_3^-] mixtures for the various compositions investigated. It can be seen that for both systems there is a tendency for non-ideal mixing, i.e., the structure of the solution depends somewhat upon composition. For both mixtures the position of the first peak in the BMIM-BMIM

g(r) moves to greater separation with increasing dilution (by HNO_3). For HNO_3/[BMIM][DCA] the magnitude of the first peak also decreases with increasing dilution. The behavior observed in Figure 2 might be associated with strong BMIM-HNO_3 interactions, but Figure 3, which show the BMIM-HNO_3 radial distribution functions for the two mixtures at selected compositions, indicate that this is not the case. For the HNO_3/[BMIM][DCA] mixtures a slight decrease (as opposed to an expected increase) in the magnitude of the first peak in the BMIM-HNO_3 radial distribution function with dilution by HNO_3 can be seen. Both mixtures show near ideal mixing behavior with respect to BMIM-HNO_3 interactions, i.e., very little composition dependence is observed in the radial distribution functions.

We have also investigated the role of HNO_3 on interactions between cations and anions in the mixtures by examining the cation-anion radial distribution functions as shown Figures 4a,b for HNO_3/[BMIM][DCA] and HNO_3/[BMIM][NO_3^-], respectively. The latter shows remarkably little influence of the oxidizer on cation-anion correlation in [BMIM][NO_3], while the former indicates that introduction of HNO_3 promotes stronger nearest-neighbor (first radial distribution function peak) interaction between BMIM and DCA. Examination of the anion-oxidizer radial distribution functions, shown in Figures 5, shows very little dependence of the nature of the DCA/HNO_3 interaction on composition, while NO_3^- /HNO_3 interactions become somewhat stronger with increasing dilution. These effects are manifested in DCA-DCA pair distribution functions that are essentially independent of composition while NO_3^-/NO_3^- correlations decrease notably with increasing HNO_3 content, as shown in Figures 6a-b.

From the magnitude of the first peaks in the radial distribution functions, it is clear that the oxidizer interacts more strongly with the anions (DCA or NO_3^-) than with the BMIM cation. Interestingly the first peak in the HNO_3/NO_3^- radial distribution function is high and narrow, indicating a strong preference for specific distance and/or orientations, while that for HNO_3/DCA is

quite broad, indicating less structure in this interaction. Atomically, the preferred interaction between HNO_3 and NO_3^- is between the acidic proton and the oxygen atoms of the anion, while for HNO_3 and DCA the preferred interaction is between the acidic proton and the (terminal) nitrogen atoms of the cyano groups. The H(acidic)-O(anion) and H(acidic)-N(cyano) atomic radial distribution functions are shown in Figure 7. Interestingly, remarkably little dependence of these interactions on the composition of the solution is observed. All radial distribution functions show a sharp, high peak at a separation of around two Å. We note that the force field employed in the simulations does not allow for transfer of the proton between species, so the nature of this interaction (e.g., minimum energy position/radial distribution function peak position) is driven entirely by physical (van der Waals and electrostatic) interactions. Integration of the radial distribution functions and multiplication by the appropriate densities yields the running coordination number of acidic protons near O(anion) or N(cyano) as shown in Figure 7c. We take a separation of 2.9 Å (see Figures 7a-b) as corresponding to the first coordination shell of acidic protons hear O(anion) or N(cyano). As expected, the number of acidic hydrogen atoms coordinating each O(anion) or N(cyano) increases with increasing dilution. For the X_{IL} = 0.2 solutions (80 mol% HNO_3) the NO_3^- oxygen atoms and DCA cyano nitrogen atoms are fully coordinated, i.e., there is more than one on average of acidic hydrogen atoms in the first coordination shell of these atoms.

B. Density, Volume of Mixing and Heat of Mixing

The density and excess volume for the two HNO_3/IL mixtures from simulations are shown in Figures 8a-b as a function of composition. The density of the pure ionic liquids are 1.030 g/cm^3 and 1.137 g/cm^3 for [BMIM][DCA] and [BMIM][NO_3^-], respectively. These values are in a good agreement with experimental values of 1.041 g/cm^3 for [BMIM][DCA][6] and 1.131 g/cm^3 for [BMIM][NO_3^-][7] with 0.5% and 1.1% deviation, respectively. The simulated density of the pure HNO_3

at 298 K is 1.45 g/cm^3, compared with an experimental density[22] of 1.51 g/cm^3. Mixing of the ILs with increasing concentration of oxidizer results in a monotonic increase in density. Examination of the excess volume of mixing shows minimal deviation from ideal mixing behavior, particularly for the HNO_3/[BMIM][NO_3^-] system. Figure 8c shows the enthalpy of mixing as a function of composition for both IL mixtures. Both exhibit exothermic behavior, with the HNO_3/[BMIM][NO_3^-] system showing stronger exothermic character. Combined with the near-ideal entropy of mixing (configurational entropy) behavior revealed by the intermolecular radial distribution functions above, we can anticipate that both of these ILs are consoluble with HNO_3. It is also clear that the temperature of the systems will increase upon adiabatic mixing, which is an important (if not crucial) aspect for onset of ignition in hypergolic mixtures. The extent of adiabatic heating for these mixtures is addressed in Section IV.

C. Self-diffusion Coefficients

The rate at which a liquid fuel and oxidizer intermix is important in determining the hypergolic character of the mixture. While intermixing dynamics are investigated in more detail below, it is instructive to examine the self-diffusion coefficients of the IL components and the oxidizer as a function of mixture composition as shown in Figure 9. Figure 9 reveals that ion self-diffusion rates are significantly greater in [BMIM][DCA] than in the [BMIM][NO_3^-], consistent with the relative viscosities of these ILs with [BMIM][NO_3^-] being about factor 4 more viscous than [BMIM][DCA] at 333K.[6,23] The HNO_3 liquid has a much lower viscosity/greater self-diffusion coefficient than the ILs, hence, dilution of the ILs with HNO_3 results in a monotonic increase in ion self-diffusion coefficients and monotonic decrease in HNO_3 diffusion coefficient. The composition dependence of the ion and HNO_3 diffusion coefficients is greater in the HNO_3/[BMIM][NO_3^-] mixture than observed in HNO_3/[BMIM][DCA] mixture. To first order this is consistent with the greater

difference in self-diffusion coefficients of HNO_3 (fast) compared to the IL (slow) in the former system compared to the latter.

IV. Simulation of Ionic Liquid/Oxidizer Mixing

In addition to analysis of bulk properties under equilibrium conditions discussed above we have investigated properties of mixtures during the mixing process. Below we discuss the analysis of interdiffusion and adiabatic heating processes upon mixing.

A. Diffusion

Fig. 10a shows the concentration profile for HNO_3 and the IL the HNO_3/[BMIM][DCA] system after 200 ps of mixing and after 3.5 ns of mixing, while Fig. 10b shows the composition profile after the same periods. Similarly, Fig. 11a shows the concentration profile for HNO_3 and the IL the HNO_3/[BMIM][NO_3^-] system after 200 ps of mixing, after 3.0 ns of mixing and after 5.9 ns of mixing, while Fig. 11b shows the composition profile after the same periods. Each profile is an average of three profiles (e.g., the 200 ps profiles are averages of profiles at 100 ps, 200 ps and 300 ps). Examination of Figs. 10 and 11 show obvious asymmetry in mixing at the interface, indicating that the mutual diffusion coefficient D_{AB} (A = oxidizer, B = IL) is strongly composition dependent for both mixtures. A typical diffusion coefficient in these mixtures might be on the order of $1x10^{-9}$ m^2/s (see Fig. 9), implying mixing on a nanometer length scale on a nanosecond time scale, consistent with behavior observed in Figs. 10 and 11.

The governing equation for mutual diffusion (Fick's second law) in one spatial dimension is given as[24]

$$\frac{\partial c_A(r,t)}{\partial t} = \frac{1}{r^m}\frac{\partial}{\partial r}\left(r^m D_{AB}(X_A)\frac{\partial c_A(r,t)}{\partial r}\right) \qquad (1)$$

$$\frac{\partial c_B(r,t)}{\partial t} = \frac{1}{r^m}\frac{\partial}{\partial r}\left(r^m D_{AB}(X_A)\frac{\partial c_B(r,t)}{\partial r}\right) \qquad (2)$$

$$X_A = \frac{c_A(r,t)}{c_A(r,t) + c_B(r,t)} \qquad (3)$$

where m = 0 for the slab geometry and 2 for spherical geometry. The dependence of D_{AB} on composition is a priori unknown and there is no robust theory for predicting $D_{AB}(X_A)$. However, it has been observed that the following relationship

$$\log D_{AB} = \log D_B + X_A(\log D_A - \log D_B) \qquad (4)$$

where D_A and D_B are the pure component self-diffusion coefficients works well in some materials. Note that the self-diffusion coefficients of the species in the mixtures tend to follow (at least reasonably) this relationship (see Fig. 9). Using the profiles at 200 ps as initial conditions, we employed eqs. 1-4 to predict the concentration and composition profiles for both mixtures. Comparisons can be seen in Figs. 10 and 11, indicating that eq. 4 provides a reasonable description of the composition dependence of D_{AB}. Here we took the self-diffusion coefficient of pure HNO_3 from Figure 9 and used the average of the cation and anion self-diffusion coefficients for the pure IL self-diffusion coefficients, again taken from Figure 9.

Once the composition dependence of the mutual diffusion coefficient is known, it is possible to utilize eqs. 1-4 with suitable initial and boundary conditions to prediction the concentration/composition profiles for any geometry of interest after any time of interest. For example, Fig. 12 shows the interfacial composition for a 2.5 mm radius droplet of [BMIM][DCA] and [BMIM][NO_3^-], respectively, in a sea of HNO_3 oxidizer, after periods of 10 and 100 ms. For both mixtures the interfacial region is on the order of microns in thickness as expected given the magnitude of the mutual diffusion coefficient (eq. 4). It is notable that on these time scales the width of the interfacial region is not significantly larger for the HNO_3/[BMIM][DCA] mixture than

for the HNO_3/[BMIM][NO_3^-] mixture, despite the fact that the self-diffusion coefficient for [BMIM][DCA] is almost four times greater than that for [BMIM][NO_3^-]. However, if we utilize an imaginary "fast" oxidizer with a self-diffusion coefficient four times that of HNO_3, mixing with [BMIM][NO_3^-] on these time scales occurs much more rapidly, as shown in Figure 12.

B. Adiabatic Heating

Heat generation upon mixing is another important property that can influence kinetics of initial reactions and, hence, the hypergolicity of the mixture. Two approaches were applied for calculating heat generation due to mixing. First, calculations were based on bulk mixture heat of mixing data (see Section III.B). If one knows the heat of mixing for the mixture of two components (i.e., IL and oxidizer) then the heat generated upon their mixing can be estimated knowing the final composition of the mixture. For example, for the [BMIM][DCA]/HNO_3 system with composition used in non-equilibrium simulations (X_{IL} = 0.23) we estimate about 17 degrees temperature increase. For [BMIM][NO_3]/HNO_3 with similar composition the corresponding heating is estimated to be about 45 degrees.

Alternatively one can conduct brute force simulations of mixing process in the NVE ensemble and directly measure how much the system heats up. While conceptually this method is straightforward, special care must be taken to control the integration uncertainty, which can otherwise lead to additional heat generation due to Hamiltonian drift. The latter can be measured by conducting simulations of a completely mixed state using the same simulation set up/parameters as in production run. A relatively short run (300-500ps) provides a good estimate of the rate of the Hamiltonian drift (if any) that can be then taken into account (subtracted) in the analysis of the production mixing simulation. Using this approach and applying correction for the Hamiltonian drift, a 17 degree heating was obtained from the non-equilibrium simulation of [BMIM][DCA]/HNO_3 mixing, consistent with the estimate from bulk simulations discussed above.

Similarly, the heating in [BMIM][NO_3]/HNO_3 system was found to be 45 degrees which is also consistent with the estimate from bulk simulations.

These simulations/estimations of heat generation due to physical mixing show that the heating is modest. In principle, taking into account that HNO_3 vaporization temperature is 353 K then even 20-40 degrees heating can be important. However, it is important to realize that the relatively narrow intermixing region is surrounded by the large amount of pure IL and oxidizer phases that can serve as heat sinks. In this case, the heating of the mixed layer will strongly depend on the interplay between thermal and molecular diffusivities in the system. The latter can be characterized by the Lewis number (Le) and is the ratio of the thermal diffusivity of a fluid, given as $\alpha = \kappa/(Cp*\rho)$, to the molecular diffusivity. Taking into account typical values for thermal conductivity (κ), heat capacity (Cp), and density (ρ) reported in the literature for IL[25] and nitric acid[26] we can estimate α for our mixture components. The thermal diffusivity of nitric acid is around $9x10^{-8}$ m^2/s, while that for a number of various ILs is in the range of $6x10^{-8}$ m^2/s. Hence, unlike molecular (mutual or self) diffusivity, we anticipate that the thermal diffusivity of the ionic liquid/nitric acid mixture will not depend strongly on composition, and will be on the order of $6x10^{-8}$ m^2/s. Using a representative diffusion coefficient of the IL/nitric mixtures of $1x10^{-9}$ m^2/s (which is on the high side of the range), we estimate $Le \geq 60$. Hence, for viscous fluids such as ILs investigated here, the time scale of thermal diffusion is much less than that of mass diffusion. Even for nitric acid itself we estimate $Le \sim 10$.

This analysis indicates that it is unlikely that any noticeable local temperature rise can be expected in the interfacial region due to heat of mixing. In our brute force mixing simulations we have analyzed the local temperature profile after 200-500ps. On these time scales, IL and HNO_3 have only intermixed in a relatively small region of 2nm wide. If the thermal dissipation would be much slower than molecular diffusion then we should observe an increase of temperature in the

intermixed region due to heat of mixing. However, neither of two mixtures showed any indication of increased temperature in the intermixed region compared to the rest of the system, indicating that the thermal energy generated due to mixing quickly dissipates to IL and HNO_3 phases and results in homogeneous heating of the entire system.

V. Conclusions

Atomistic molecular dynamics simulations of HNO_3/[BMIM][NO_3^-] and HNO_3/[BMIM][DCA] mixtures using polarizable force field revealed a complete consolubility for both systems in the entire range of concentrations. Both mixtures exhibited exothermic behavior, with the HNO_3/[BMIM][NO_3^-] system showing stronger exothermic character. Analysis of various pair correlations functions showed very little dependence on mixture composition indicating a near-ideal entropy of mixing. Analysis of the liquid structure revealed that the most prominent difference between two mixtures is in the anion-HNO_3 correlations. The first peak in the HNO_3/NO_3^- radial distribution function is high and narrow, indicating a strong preference for specific distance and/or orientations, while that for HNO_3/DCA is quite broad, indicating less structure in this interaction. However, in both systems the potential anion proton acceptor atoms (oxygens for NO_3^- and nitrogens in DCA) are well coordinated by acidic hydrogen at all investigated compositions indicating that there no structural hindrances for initial anion protonation reactions to occur.

Analysis of molecular diffusivity showed a significant speed up of mobility of ions upon dilution with nitric acid. We found that molecular interdiffusion obtained from brute force simulation of mixing IL and oxidizer can be accurately described by a simple diffusion equation utilizing parameters obtained from MD simulations and simple empirical relation for calculation of mutual diffusion coefficients. The developed continuum level analytical model allowed us to estimate concentration profiles on time and length scales relevant to hypergolic ignition (multiple

ms and μm) but are well outside of accessibility range for brute force atomistic MD simulations. Our analysis indicates that despite quite different diffusivity/viscosity between two investigated ILs their intermixing with nitric acid is quite similar on time scales of 10-100ms. Finally, the analysis of adiabatic heating upon mixing IL and oxidizer revealed that the released enthalpy of mixing is sufficient to allow a noticeable heating in the intermixed region. However, due to intrinsically high thermal diffusivity (compared to molecular diffusivity) of IL and nitric acid all heat generated in the intermixed layer is quickly dissipating to non-mixed regions. Taking into account that on time scales 10-100ms only a small fraction of a fuel droplet has intermixed with an oxidizer and hence the dominating non-mixed regions of IL and oxidizer can quickly sink the heat generated in the intermixed region. Therefore, no noticeable temperature increase due to heat of mixing can be expected in the intermixing region.

VI. Acknowledgment

We are grateful for the financial support of this work by the Air Force Office of Scientific Research and through the SBIR program (contract number FA9300-11-C-3012) to Wasatch Molecular Inc. Opinions, interpretations, conclusions, and recommendations are those of the authors and are not necessarily endorsed by the United States Government.

References.

[1] Y. Zhang, H. Gao, Y-H. Joo, and J.M. Shreeve, Angew. Chem. Int. Ed. **50**, 9554-9562 (2011).

[2] S.D. Chambreau, S. Schneider, M. Rosander, T. Hawkins, C.J. Gallegos, M.F. Pastewait, and G.L. Vaghjiani, J. Phys. Chem. A **112**, 7816 (2008).

[3] S. Shneider, T. Hawkins, M. Rosander, G.L. Vahjiani, S. Chambreau, and G. Drake, Energy & Fuels, **22**, 2871 (2008).

[4] A.J. Alfano, J.D. Mills, and G.L. Vaghjiani, Rev. Scientific Instrum. **77**, 045109 (2006).

[5] V.N. Emel'yanenko, S.P. Verevkin, A. Heintz, and C. Schick, J. Phys. Chem. B **112**, 8095 (2008).

[6] C.P. Fredlake, J.M. Crosthwaite, D.G. Hert, S. Aki, and J.F. Brennecke, J. Chem. Eng. Data**, 49,** 954 (2004).

[7] K.R. Seddon, A. Stark, and M.J. Torres, Clean Solvents **819**, 34 (2002).

[8] L.A. Blanchard, Z.Y. Gu, and J.F. Brennecke, J. Phys. Chem. B **105***,* 2437 (2001).

[9] V.N. Emel'yanenko, S.P. Verevkin, and A Heintz, A. J. Am. Chem. Soc. **129**, 3930 (2007).

[10] S. Chambreau, G.L. Vaghjiani, A. To, C. Koh, D. Strasser, O. Kostko, and S.R. Leone, S. R. J. Phys. Chem. B **114**, 1361 (2010).

[11] D. Bedrov and O. Borodin, J. Phys. Chem. B **114**, 12802 (2010).

[12] N.M. Micaelo, A.M. Baptista, and C.M. Soares, J. Phys. Chem. B **110,** 14444 (2006).

[13] S.V. Sambasivarao, and O. Acevedo, J. Chem. Theory Comput. **5,** 1038 (2009).

[14] M.H. Kowsari, S. Alavi, M. Ashrafizaadeh, and B. Najafi, J. Chem. Phys. **129**, 224508 (2008).

[15] M.H. Kowsari, S. Alavi, M. Ashrafizaadeh, and B. Najafi,. J. Chem. Phys. **130**, 014703 (2009).

[16] G. Feng, J.S. Zhang, and R. Qiao, J. Phys. Chem. C **113**, 4549 (2009).

[17] J. Wang, and G.A. Voth, J. Am. Chem. Soc. **127**, 12192 (2005).

[18] C. Cadena, and E. J. Maginn, J. Phys. Chem. B 110, 18026 (2006).

[19] O. Borodin, O. J. Phys. Chem. B **113**, 11463 (2009).

[20] B.J. Palmer, J. Comput. Phys **104**, 470 (1993).

[21] G.J. Martyna, M.E. Tuckerman, D.J. Tobias, and M.L. Klein, Mol. Phys. **87**, 1117 (1996).

[22] Sibbitt, W. L.; St. Clair, C. R.; Bump, T. R.; Pagerey, P. F.; Kern, J. P.; Fyfe, D. W. *Nat. Adv. Comm. for Aeronaut. Tech. Note. 2970*, **1953**. (Accessed via: Sibbit, W L. *Physical properties of concentrated nitric acid*. UNT Digital Library. http://digital.library.unt.edu/ark:/67531/metadc56640/.)

[23] M. Engelmann, H. Schmidt, J. Safarov, J. Nocke, and E. Hassel, Acta Chimica Slovaca, 5, 86, (2012).

[24] Darrel R. Tenney and Jalaiah Unnan, Nasa Technical Paper 1281, "Effect of Concentration Dependence on the Diffusion Coefficient on the Homogenization Kinetics in Multiphase Binary Allow Systems", (1978).

[25] C. Frez, G.J.; Diebold, C.D. Tran, and S. Yu, J. Chem. Eng. Data **51** , 1250-1255 (2006).

[26] A. J.-J. Kadjo, J.-P. Maye1, J. Saillard, G. Thévenot, J.-P. Garnier, and S. Martemianov, "Measurement of Thermal Conductivity and Diffusivity of Electrically Conducting and Highly Corrosive Liquids from Small Samples with a New Transient Hot-Wire Instrument " Proceeding of 5th European Thermal Sciences Conference 18-22 May 2008, Eindhoven, the Netherlands (2008).

Figure Captions.

Figure 1. Chemical structure of ions and nitric acid as well as snapshots from equilibrium bulk simulation and non-equilibrium mixing simulation of [BMIM][DCA]/nitric acid system.

Figure 2. BMIM-BMIM radial distribution functions for HNO_3/[BMIM][DCA] (a) and HNO_3/[BMIM][NO_3^-] (b) mixtures.

Figure 3. BMIM-HNO_3 radial distribution functions for HNO_3/[BMIM][DCA] and HNO_3/[BMIM][NO_3^-] mixtures at selected compositions.

Figure 4. Cation-anion radial distribution functions for HNO_3/[BMIM][DCA] (a) and HNO_3/[BMIM][NO_3^-] (b) mixtures.

Figure 5. Anion-HNO_3 radial distribution functions for HNO_3/[BMIM][DCA] and HNO_3/[BMIM][NO_3^-] mixtures at selected compositions.

Figure 6. Anion-anion radial distribution functions for HNO_3/[BMIM][DCA] (a) and HNO_3/[BMIM][NO_3^-] (b) mixtures.

Figure 7. The H(acidic)-O(anion) and H(acidic)-N(cyano) atomic radial distribution functions for HNO_3/[BMIM][NO_3^-] (a) and HNO_3/[BMIM][DCA] (b), along with the corresponding running coordination numbers (c).

Figure 8. Density (a), excess volume (b) and heat of mixing (c) for HNO_3/[BMIM][DCA] and HNO_3/[BMIM][NO_3^-] mixtures as a function of composition.

Figure 9. Ion and oxidizer self-diffusion coefficients as a function of mixture composition for HNO_3/[BMIM][DCA] and HNO_3/[BMIM][NO_3^-] mixtures.

Figure 10. Time-dependent composition (a) and concentration (b) profiles for the HNO_3/[BMIM][DCA] slab system after 200 ps and 3.5 ns of mixing.

Figure 11. Time-dependent composition (a) and concentration (b) profiles for the HNO_3/[BMIM][NO_3^-] slab system after 200 ps, 3.0 ns and 5.9 ns of mixing.

Figure 12. Interfacial profiles for a 2.5 mm radius sphere of [BMIM][DCA] or [BMIM][NO_3^-] (indicated by arrows) in a sea of HNO_3 predicted by using eqs. 1-4. The "fast" oxidizer system shows mixing of [BMIM][NO_3^-] with an oxidizer than has a self-diffusion coefficient four times that of HNO_3.

Figure 1.

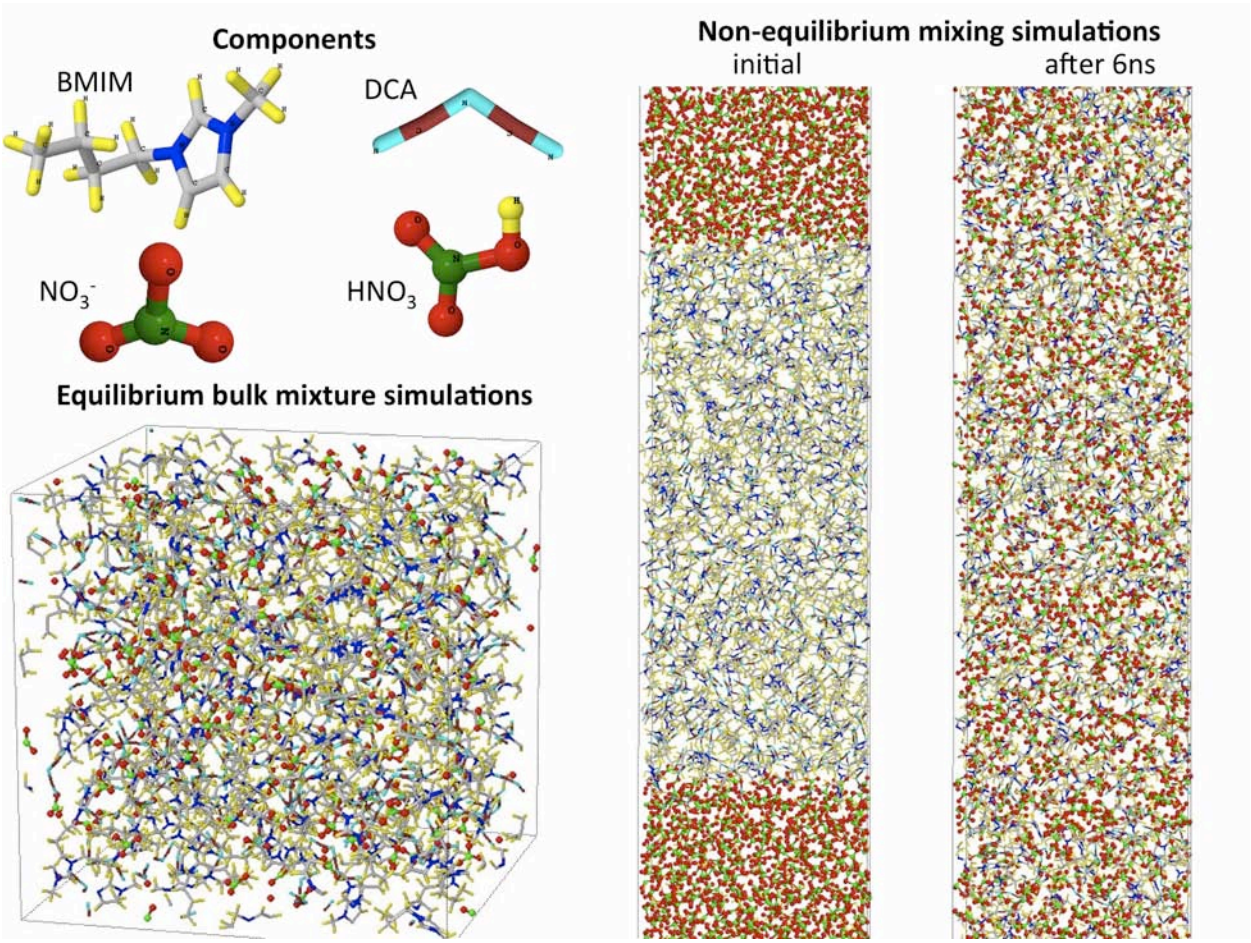
Components
BMIM
DCA
NO_3^-
HNO_3
Equilibrium bulk mixture simulations
Non-equilibrium mixing simulations
initial
after 6ns

Figure 2.

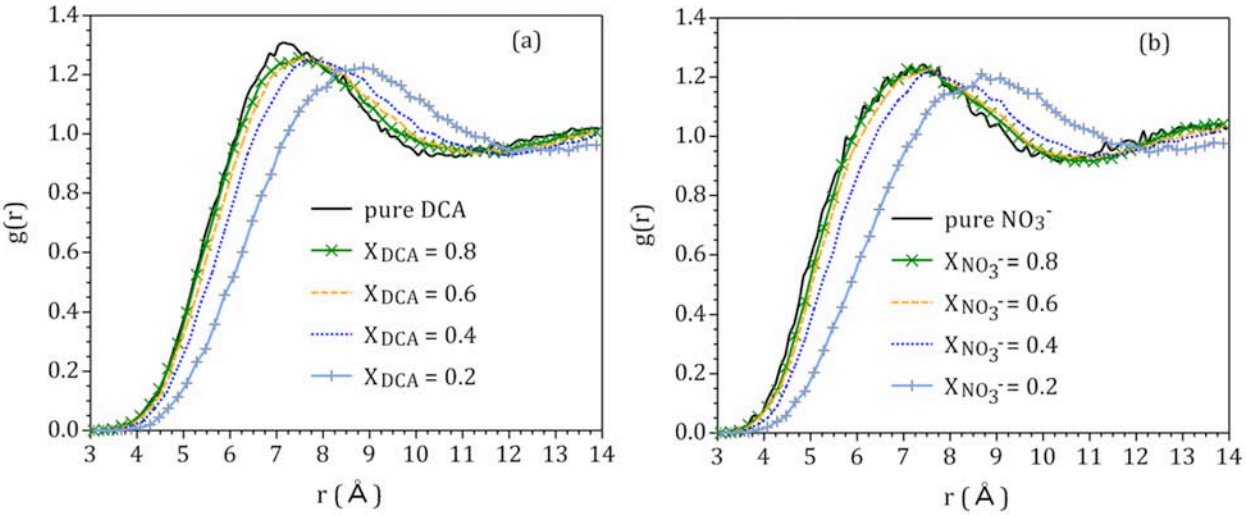
(a)
g(r)
r (Å)
pure DCA
X_DCA = 0.8
X_DCA = 0.6
X_DCA = 0.4
X_DCA = 0.2
(b)
g(r)
r (Å)
pure NO3-
X_NO3- = 0.8
X_NO3- = 0.6
X_NO3- = 0.4
X_NO3- = 0.2

Figure 3.

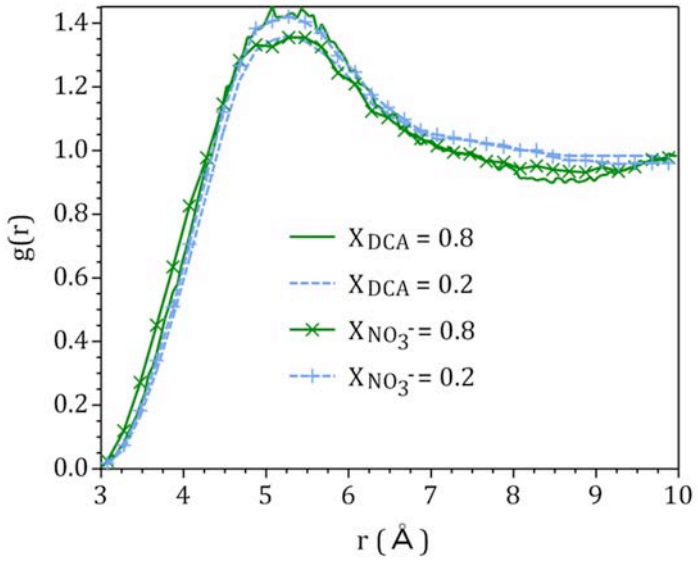

Figure 4.

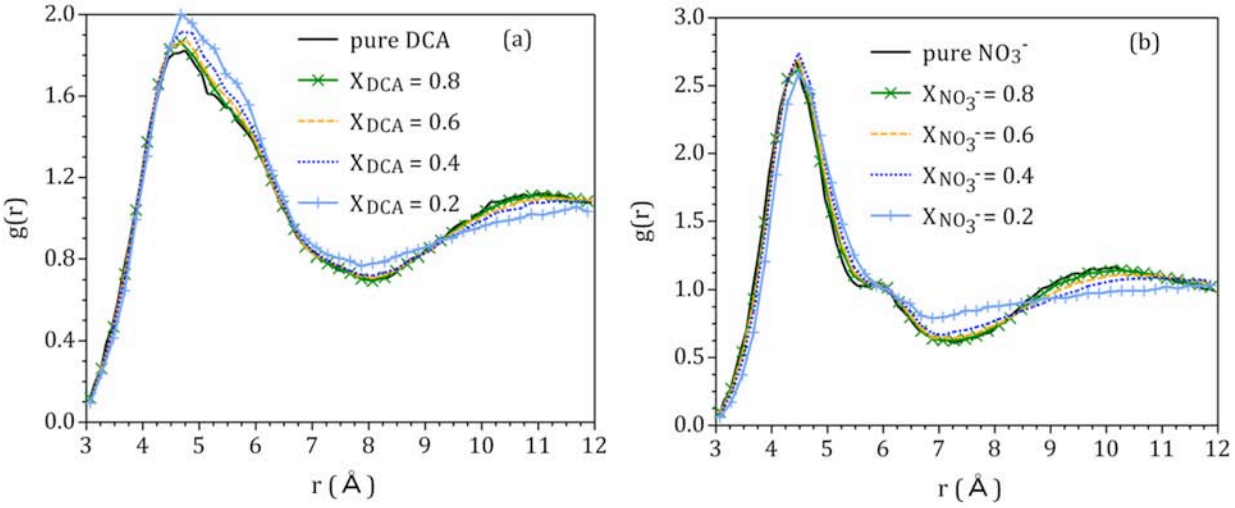
pure DCA
(a)
X_{DCA} = 0.8
X_{DCA} = 0.6
X_{DCA} = 0.4
X_{DCA} = 0.2
g(r)
r (Å)
pure NO_3^-
(b)
$X_{NO_3^-}$ = 0.8
$X_{NO_3^-}$ = 0.6
$X_{NO_3^-}$ = 0.4
$X_{NO_3^-}$ = 0.2
g(r)
r (Å)

Figure 5.

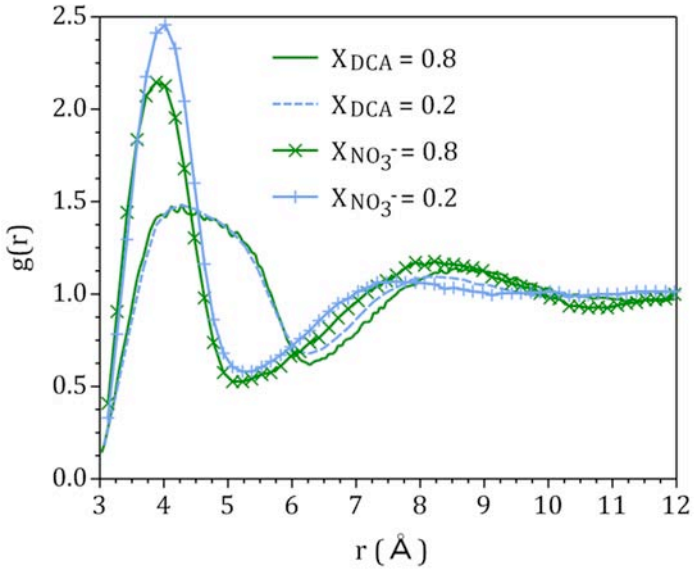
2.5
2.0
1.5
1.0
0.5
0.0
g(r)
3
4
5
6
7
8
9
10
11
12
r (Å)
X DCA = 0.8
X DCA = 0.2
X NO3- = 0.8
X NO3- = 0.2

Figure 6.

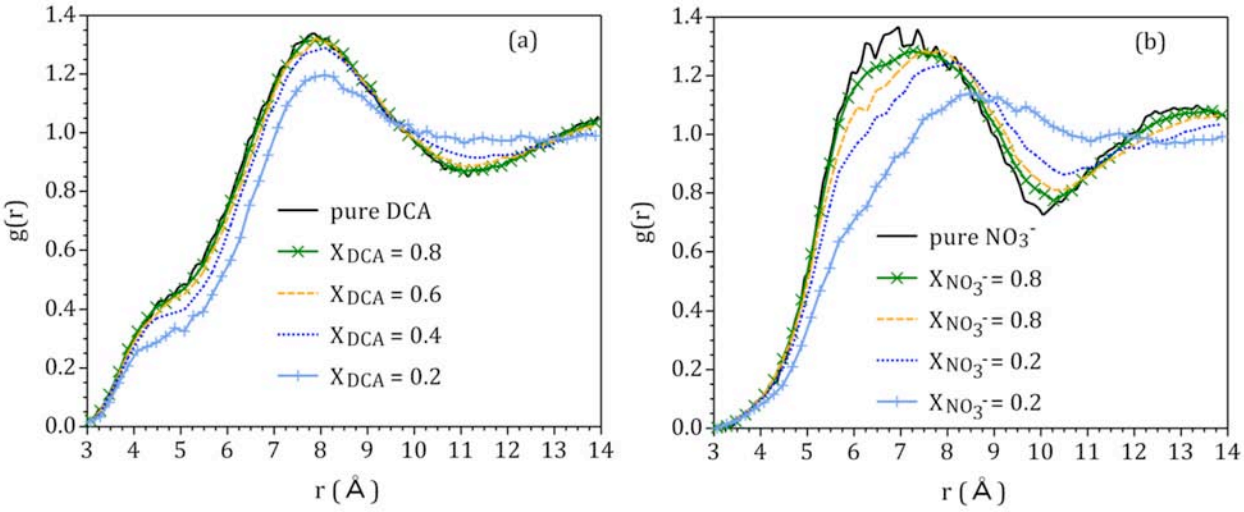
(a)
g(r)
r (Å)
pure DCA
X_DCA = 0.8
X_DCA = 0.6
X_DCA = 0.4
X_DCA = 0.2
(b)
g(r)
r (Å)
pure NO3-
X_NO3- = 0.8
X_NO3- = 0.8
X_NO3- = 0.2
X_NO3- = 0.2

Figure 7

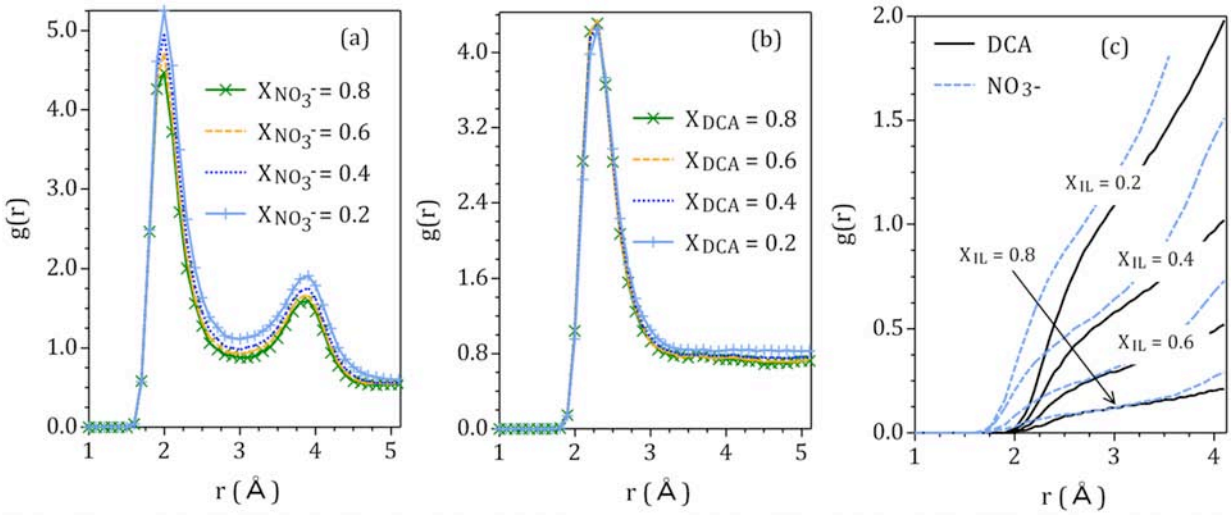
(a)
$X_{NO_3^-}$ = 0.8
$X_{NO_3^-}$ = 0.6
$X_{NO_3^-}$ = 0.4
$X_{NO_3^-}$ = 0.2
g(r)
r (Å)
(b)
X_{DCA} = 0.8
X_{DCA} = 0.6
X_{DCA} = 0.4
X_{DCA} = 0.2
g(r)
r (Å)
DCA
NO_3-
(c)
X_{IL} = 0.2
X_{IL} = 0.8
X_{IL} = 0.4
X_{IL} = 0.6
g(r)
r (Å)

Figure 8

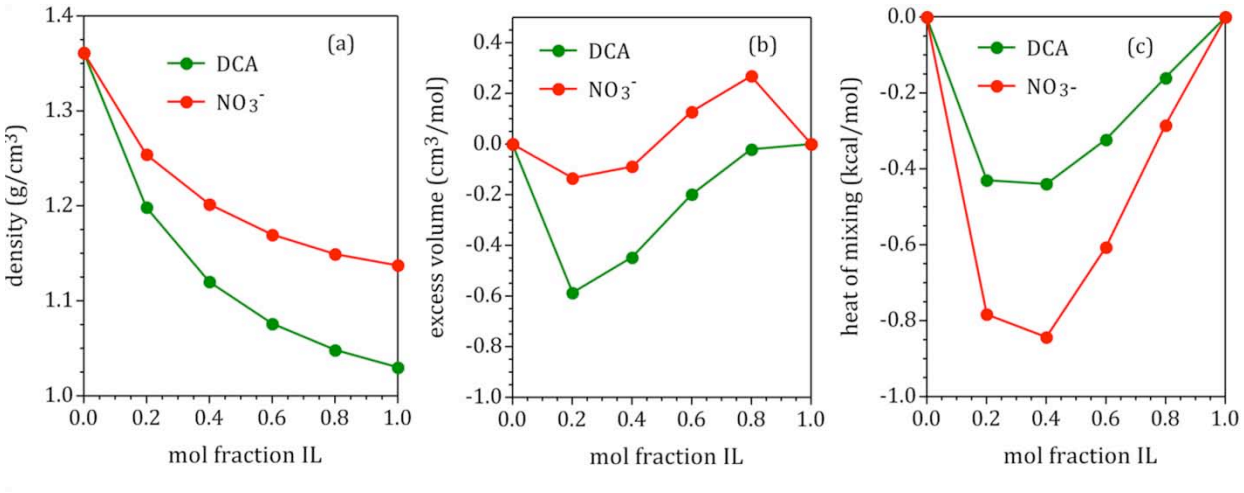
(a)
DCA
NO3-
density (g/cm3)
mol fraction IL
(b)
DCA
NO3-
excess volume (cm3/mol)
mol fraction IL
(c)
DCA
NO3-
heat of mixing (kcal/mol)
mol fraction IL

Figure 9.

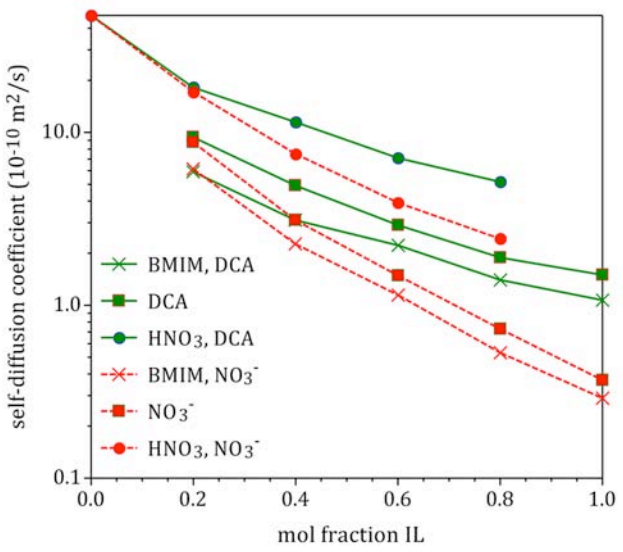
self-diffusion coefficient (10^{-10} m^2/s)
10.0
1.0
0.1
0.0
0.2
0.4
0.6
0.8
1.0
mol fraction IL
BMIM, DCA
DCA
HNO3, DCA
BMIM, NO3-
NO3-
HNO3, NO3-

Figure 10.

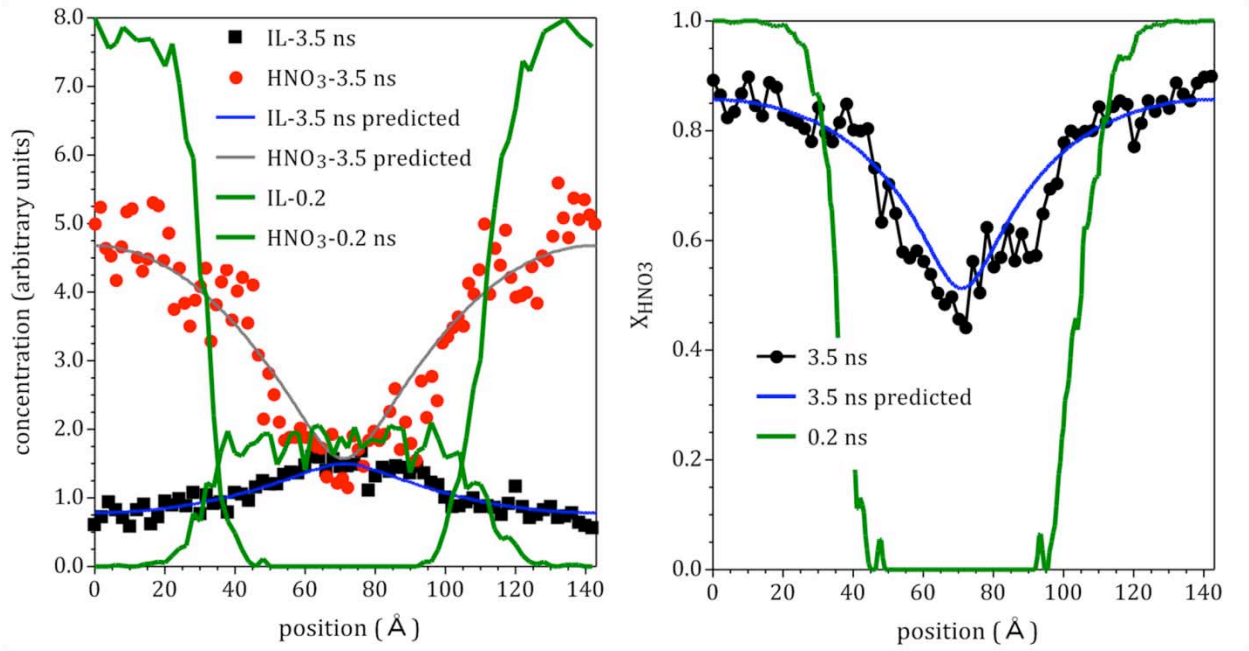
concentration (arbitrary units)
position (Å)
IL-3.5 ns
HNO3-3.5 ns
IL-3.5 ns predicted
HNO3-3.5 predicted
IL-0.2
HNO3-0.2 ns
XHNO3
3.5 ns
3.5 ns predicted
0.2 ns

Figure 11.

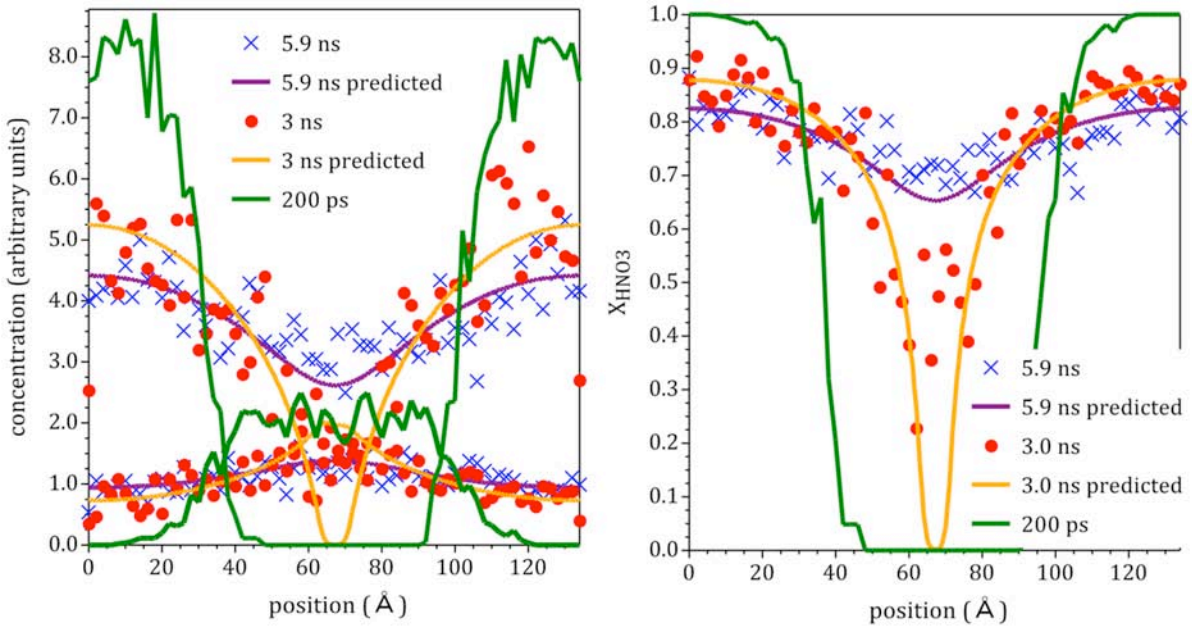
concentration (arbitrary units)
position (Å)
5.9 ns
5.9 ns predicted
3 ns
3 ns predicted
200 ps
x_{HNO3}
position (Å)
5.9 ns
5.9 ns predicted
3.0 ns
3.0 ns predicted
200 ps

Figure 12.

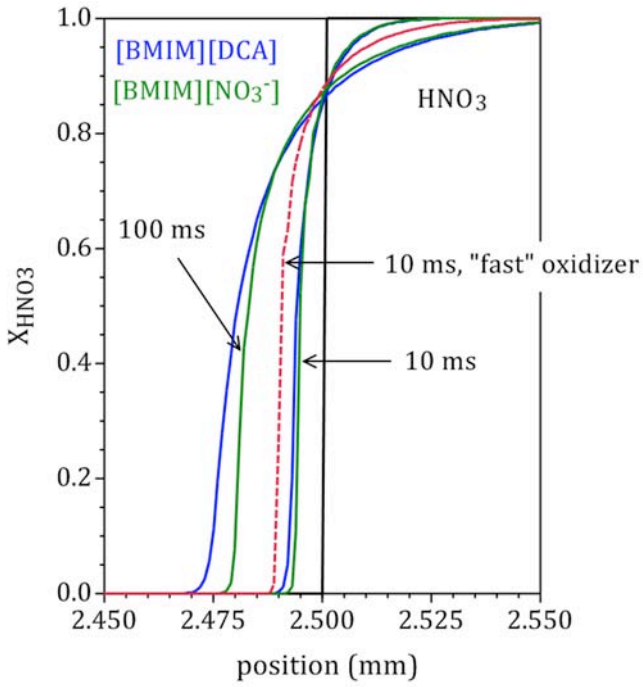
[BMIM][DCA]
[BMIM][NO3-]
HNO3
100 ms
10 ms, "fast" oxidizer
10 ms
XHNO3
position (mm)
1.0
0.8
0.6
0.4
0.2
0.0
2.450
2.475
2.500
2.525
2.550